AD-A113 005 DAVID W TAYLOR NAVAL SHIP RESEARCH AND DEVELOPMENT CE--ETC F/G 20/4
COMPUTATION OF RELATIVE MOTION OF SHIPS TO WAVES.(U)
MAR 82 C M LEE

UNCLASSIFIED DTNSRDC-82/019 NL

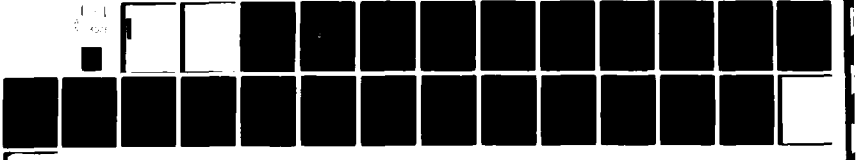

END
DATE FILMED
4 82
DTIC

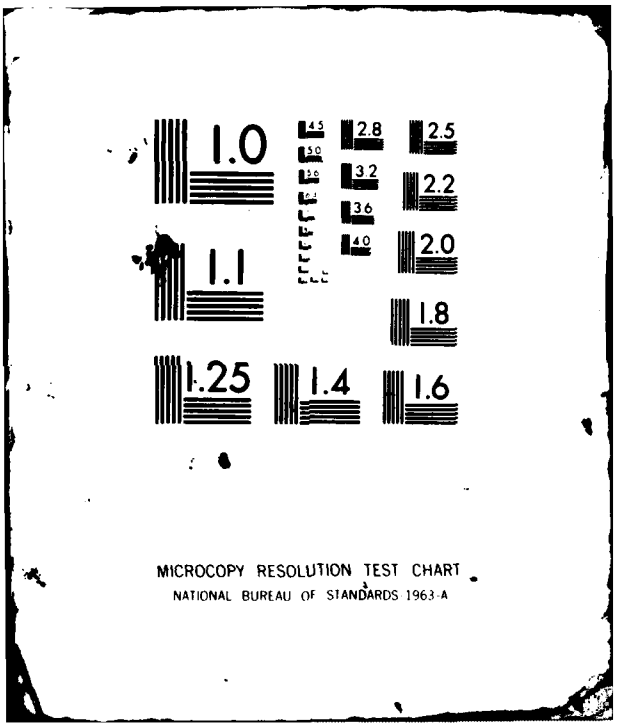
1.0
1.1
1.25
1.4
1.6
2.8
3.2
3.6
4.0
2.5
2.2
2.0
1.8
MICROCOPY RESOLUTION TEST CHART
NATIONAL BUREAU OF STANDARDS 1963-A

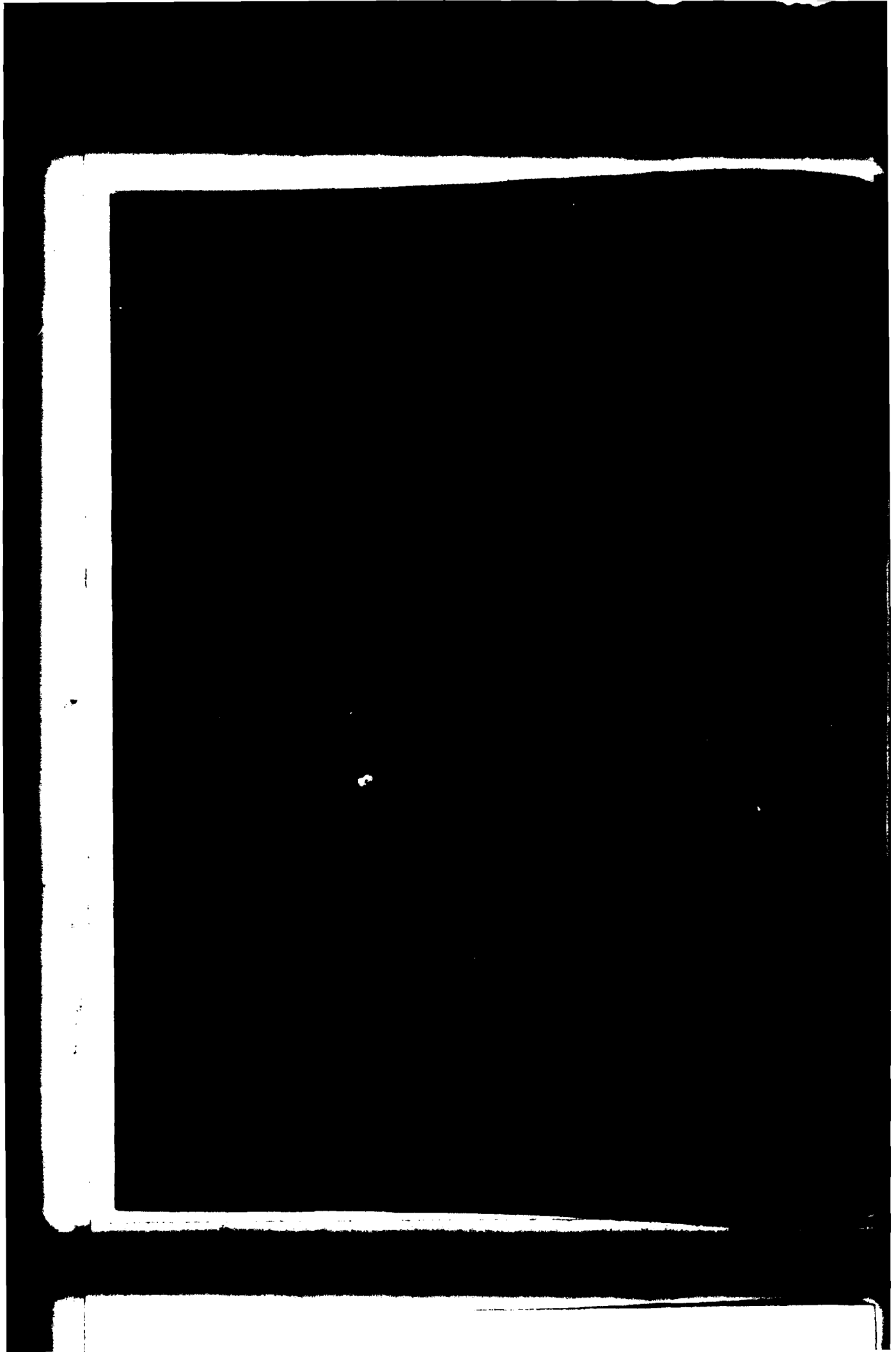

UNCLASSIFIED

SECURITY CLASSIFICATION OF THIS PAGE (When Data Entered)

REPORT DOCUMENTATION PAGE		READ INSTRUCTIONS BEFORE COMPLETING FORM
1. REPORT NUMBER DTNSRDC-82/019	2. GOVT ACCESSION NO. AD-A113 005	3. RECIPIENT'S CATALOG NUMBER
4. TITLE (and Subtitle) COMPUTATION OF RELATIVE MOTION OF SHIPS TO WAVES		5. TYPE OF REPORT & PERIOD COVERED Formal 6. PERFORMING ORG. REPORT NUMBER
7. AUTHOR(s) Choung M. Lee		8. CONTRACT OR GRANT NUMBER(s)
9. PERFORMING ORGANIZATION NAME AND ADDRESS David W. Taylor Naval Ship Research and Development Center Bethesda, Maryland 20084		10. PROGRAM ELEMENT, PROJECT, TASK AREA & WORK UNIT NUMBERS Program Element 61153N Task Area SR023010= Work Unit 1561-014
11. CONTROLLING OFFICE NAME AND ADDRESS		12. REPORT DATE March 1982 13. NUMBER OF PAGES 24
14. MONITORING AGENCY NAME & ADDRESS(if different from Controlling Office)		15. SECURITY CLASS. (of this report) UNCLASSIFIED 15a. DECLASSIFICATION/DOWNGRADING SCHEDULE

16. DISTRIBUTION STATEMENT (of this Report)

APPROVED FOR PUBLIC RELEASE: DISTRIBUTION UNLIMITED

17. DISTRIBUTION STATEMENT (of the abstract entered in Block 20, if different from Report)

18. SUPPLEMENTARY NOTES

19. KEY WORDS (Continue on reverse side if necessary and identify by block number)

Ship motion in waves, radiated waves, relative motion, strip theory, diffracted waves

20. ABSTRACT (Continue on reverse side if necessary and identify by block number)

An analytical method is developed for predicting the vertical motion of a point on a ship relative to the motion of the free surface. The prediction method presented here takes into account the effect of the deformation of the incident waves on the relative motion. The causes of the deformation considered are the waves generated by diffraction and the

(Continued on reverse side)

DD FORM 1 JAN 73 1473 EDITION OF 1 NOV 65 IS OBSOLETE
S/N 0102-LF-014-6601

UNCLASSIFIED

SECURITY CLASSIFICATION OF THIS PAGE (When Data Entered)

(Block 20 continued)

waves generated by the motion of the ship. The method is based on the two-dimensional approximation of the flow around the cross sections of ships. The results reveal that the deformation of the incident waves is so significant that it should be accounted for in the prediction of the relative motion of ships.

TABLE OF CONTENTS

LIST OF FIGURES

LIST OF TABLES

NOTATION

$\bar{A}_k$	Free-surface amplitude at a point (x,y,0) per unit amplitude of oscillation in the kth mode
$\bar{A}_R$	Reflected wave amplitude per unit incident wave amplitude
$\bar{A}_W^{(I)}$	Free-surface amplitude per unit incident wave amplitude at a point on the incident side of the wave due to incident and reflected waves
$\bar{A}_W^{(L)}$	Free-surface amplitude per unit incident wave amplitude at a point on the lee side of the wave due to transmitted wave
$\bar{A}^{(I)}$	Free-surface amplitude at a point on the incident side per unit incident wave amplitude due to incident, reflected and motion-generated waves
$\bar{A}_W^{(M)}$	Free-surface amplitude per unit incident wave amplitude at a point (x,y,0) due to combined sway, heave, and roll motion
$A_{k\ell}$	Added mass in the kth mode due to motion in the ℓth mode
b	Half-beam of a cross section at the calm waterline
$B_{k\ell}$	Damping (due to wave making) coefficient in the kth mode due to motion in the ℓth mode
$C_{k\ell}$	Restoring coefficient (spring constant) in the kth mode due to motion in the ℓth mode
$F_k^{(e)}$	Wave-excited force or moment in the kth mode
g	Gravitational acceleration
$j = \sqrt{-1}$	Imaginary unit
$K = \lambda/2\pi$	Wave number
$\underline{N}$	Two-dimensional unit normal vector
$\underline{n}$	Unit normal vector on the body surface pointing into the body
O,x,y,z	Right-handed Cartesian coordinate system (see Figure 1)
U	Forward velocity of ship

$\zeta(x,y,t)$	Free-surface elevation
ζ_A	Incident wave amplitude
λ	Wave length
μ	Wave heading angle; $\mu = 0$ for following wave
$\overline{\xi}_k$	Complex amplitude of displacement of body due to oscillation in the kth mode
$\xi_R(x,y,z,t)$	Vertical displacement of a point (x,y,z) on a body relative to the point on the free surface on the same vertical line (see Equation (6))
$\xi_V(x,y,z,t)$	Vertical displacement of a point (x,y,z) on a body due to motion
ρ	Density of water
$\Phi(x,y,z,t)$	Velocity potential function which represents the total fluid disturbance due to wave and body motion
$\phi_D(x,y,z)$	Complex velocity potential for diffracted wave
$\phi_I(x,y,z)$	Complex velocity potential for incident wave
$\phi_k(x,y,z)$	Complex velocity potential for forced oscillation in the kth mode
$\phi_k'(y,z,x)$	Two-dimensional complex velocity potential
$\phi_s(x,y,z)$	Velocity potential for disturbance generated by the steady forward motion of a ship

COMPUTATION OF RELATIVE MOTION OF SHIPS TO WAVES

Choung M. Lee
David Taylor Naval Ship
R&D Center
Bethesda, Maryland, U.S.A.

Abstract

An analytical method is developed for predicting the vertical motion of a point on a ship relative to the motion of the free surface. The prediction method presented here takes into account the effect of the deformation of the incident waves on the relative motion. The causes of the deformation considered are the waves generated by diffraction and the waves generated by the motion of the ship. The method is based on the two-dimensional approximation of the flow around the cross sections of ships. The results reveal that the deformation of incident waves is so significant that it should be accounted for in the prediction of the relative motion of ships.

I. Introduction

The vertical motion of a point on a ship hull with respect to the undulating free surface is important information in the seakeeping investigation of ships. This motion is often called "Relative Motion." The relative motion has a direct effect on the inception of deck wetness, slamming of the ship bottom, and rudder and propeller emergence.

In general, the relative motion is computed under the assumption that the incident wave system is undisturbed. However, the incident waves can be significantly disturbed in the vicinity of a ship due to the diffraction by the ship surface and the waves generated by the motion of the ship. Hence, one can easily surmise that the cause of the poor correlation between the predicted and the measured [1,2,3] relative motion is the assumption of the undisturbed incident waves near a ship.

In this paper a method to account for the free-surface disturbance in the computation of relative motion is described. The method, as an initial attempt, is limited to a two-dimensional approximation within the context of strip theory. This approach is taken because firstly, the results can be readily incorporated into the existing computational scheme of ship motion based on strip theory[4] and secondly, an evaluation of the two-dimensional approximation ought to be made before undertaking a more complex three-dimensional approach. The strip approach of obtaining the free-surface disturbances near a ship hull was encouraged by the success achieved by strip theory in the computation of the absolute motion of ships in waves.

The two-dimensional potentials are obtained by using the method of distribution of pulsating sources on the boundary of the cross section of the body. The source distribution is extended on the waterline inside the body to remove the irregular behaviors of the potentials at certain discrete frequencies. Various cross checkings of the numerical convergence are made to ensure the validity of the computed results.

The computed results of a pontoon having a uniform cross section identical to the midship of a mariner hull form are presented. The contribution from the various sources generating local waves near the pontoon are shown in the figures. The results indicate clearly that the free surface motion at the sides of a ship should be considered if a reliable prediction of the relative vertical motion is desired. The present study will be incorporated in a strip fashion into an existing ship-motion computer program, and the validity of the presently developed method will be investigated.

II. Analysis

The coordinate system to be used in the analysis is a right-handed Cartesian coordinate system which moves on the calm-water surface in the mean course of the ship with the ship speed. The origin is located directly above the center of gravity of the ship at its mean position; the x-axis is directed toward the bow; and the z-axis is directed vertically upward; see Figure 1.

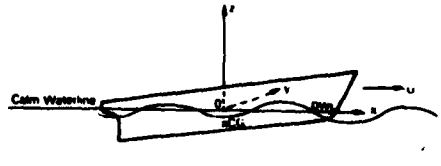

Figure 1 – Description of Coordinate System

We assume that the water is incompressible and its motion irrotational such that a velocity potential can be defined in the fluid region. We also assume that the water is infinitely deep and that no current exists.

If we denote the velocity potential which represents the disturbance of the fluid by $\phi(x,y,z,t)$, then it can be decomposed in the following form for a ship moving with a constant velocity U in a regular plane wave system,

$$\phi(x,y,z,t) = -Ux + \phi_s(x,y,z) + Re[\phi_e(x,y,z)e^{j\omega_e t}] \quad (1)$$

Here, ω_e is the wave-encounter frequency, Re means the real part of what follows, ϕ_s is the steady potential, and ϕ_e is the oscillatory complex amplitude of the oscillatory potential which can be further decomposed into

$$\phi_e = \phi_I + \phi_D + \sum_{k=1}^{6} \phi_k \bar{\xi}_k \quad (2)$$

where ϕ_I is the incident-wave potential; ϕ_D the diffracted-wave potential; ϕ_k the forced-oscillation potential in the kth mode of motion; and $\bar{\xi}_k$ the complex amplitude of the displacement of the body due to oscillation in the kth mode. The incident-wave potential ϕ_I can be given explicitly by

$$\phi_I(x,y,z) = j\frac{g\zeta_A}{\omega} e^{-jk(x\cos\mu + y\sin\mu) + Kz} \quad (3)$$

where

ω = wave frequency in radians per sec

g = gravitational acceleration

ζ_A = wave amplitude

$K = \omega^2/g = 2\pi/\lambda$ = wave number for deep water

λ = wave length

μ = wave heading angle; $\mu = 0$ is following waves

$j = \sqrt{-1}$

The free-surface elevation $\zeta(x,y,t)$ can be obtained from Bernoulli's equation in terms of the velocity potential by

$$\zeta(x,y,t) = -\frac{1}{g}\left(\frac{\partial}{\partial t} - U\frac{\partial}{\partial x}\right)\phi(x,y,0,t) + O(\phi^2)$$

$$= \frac{U}{g}\left[\phi_{sx}(x,y,0) + \phi_{ex}(x,y,0)e^{j\omega_e t}\right]^*$$

$$- j\frac{\omega_e}{g}\phi_e e^{j\omega_e t} = \zeta_s + \zeta_e e^{j\omega_e t} \quad (4)$$

where

$$\zeta_s(x,y) = \frac{U}{g}\phi_{sx}(x,y,0) \quad (4a)$$

$$\zeta_e(x,y) = \frac{1}{g}[U\phi_{ex}(x,y,0) - j\omega_e\phi_e] \quad (4b)$$

The vertical displacement of a point (x,y,z) on a ship, denoted by $\xi_v(\underline{x},t)$, is given by

$$\xi_v(\underline{x},t) = z + \xi_3(t) - x\xi_5(t) + y\xi_4(t) \quad (5)$$

where $\underline{x} = (x,y,z)$, and ξ_3, ξ_4 and ξ_5 are, respectively, the heave, roll and pitch displacement from the mean position of the body. The relative motion of a point with respect to the free surface motion at the same horizontal coordinates (x,y) is defined by

$$\xi_R(\underline{x},t) = \xi_v(\underline{x},t) - \zeta(x,y,t) \quad (6)$$

The vertical position of the point on the hull from the calm water surface at zero speed is not, of course, necessarily the same as that at a non-zero forward speed due to the sinkage and trim of the ship. In a strict sense, an inclusion of the sinkage and trim effect in the determination of the relative motion means that the second-order effects contributed by the terms such as $O(\phi_s\phi_e)$, $O(\phi_s^2)$, and $O(\phi_e^2)$ should also be included in the analysis. However, an investigation of the second-order effects will not be pursued in the present study. The analysis will be kept within the first order of the incident wave amplitude and of the slenderness parameter of the body.

Determination of Steady Free Surface

The free-surface deformation caused by a steady translation of a ship in calm water at constant speed U is obtained from the linearized Bernoulli's equation as

$$\zeta_s(x,y) = \frac{U}{g}\phi_{sx}(x,y,0) \quad (7)$$

The boundary-value problem for ϕ_s is as follows:

$$\phi_{sxx}(x,y,0) + \frac{g}{U^2}\phi_s = 0 \quad (8)$$

$$\phi_{sn}\Big|_{S_e} = \frac{\partial x}{\partial n}\Big|_{S_e} \quad (9)$$

where S_e denotes the hull surface below the calm-water surface, and $\underline{n} = (n_1,n_2,n_3)$ is the unit normal vector on S_e pointing into the body;

$$\phi_{sz}(x,y,-\infty) = 0 \quad (10)$$

and

$$\lim_{r\to\infty}\phi_s = \begin{cases} O(r^{-1/2}) & \text{for } x > 0 \\ o(1) & \text{for } x < 0 \end{cases} \quad (11)$$

where $r = \sqrt{x^2 + y^2}$

*When the spatial variables x, y, z and n (normal) are used as a subscript, it means a partial derivative with the respective variable. Also, when a complex function is multiplied by $e^{j\omega_e t}$, only the real part of the product should be realized.

To obtain the solution of the foregoing boundary-value problem, the thin-ship assumption will be used. If we represent the hull geometry by

$$y = \pm f(x,z), \tag{12}$$

then the unit normal vector on the ship hull surface pointing into the body can be determined by

$$\underline{n} = \frac{(f_x, \mp 1, f_z)}{\sqrt{1+f_x^2+f_z^2}} \quad \text{on } y = \pm f \tag{13}$$

Substitution of Equation (13) into Equation (9) yields

$$f_x \phi_{sx}(x,\pm f,z) \mp \phi_{sy} + f_z \phi_{sz} = U f_x \tag{14}$$

We assume that the ship in consideration is thin such that $f = O(\varepsilon)$ where ε is a small parameter representing the beam to length ratio of the ship. Then, from Equation (14), discarding the terms of $O(\varepsilon^2)$, we find that

$$\phi_{sy}(x,\pm 0,z) = \mp U f_x \tag{15}$$

The solution of ϕ_s is well known from thin-ship theory (see, e.g., Wehausen and Laitone[5]) and is given by

$$\phi_s(x,y,z) = \frac{U}{2\pi} \iint_{S^{(0)}} \frac{f_\xi(\xi,\zeta)}{\sqrt{(x-\xi)^2+y^2+(z-\zeta)^2}}\, d\xi d\zeta$$

$$- \frac{U}{2\pi} \iint_{S^{(0)}} \hat{G}_0(x-\xi,y,z+\zeta) f_\xi(\xi,\zeta)\, d\xi d\zeta \tag{16}$$

where $S^{(0)}$ denotes the longitudinal center-plane of the ship, and

$$\hat{G}_0(x-\xi,y,z+\zeta) = \frac{1}{\sqrt{(x-\xi)^2+y^2+(z+\zeta)^2}}$$

$$+ \frac{4g}{\pi U^2} \int_0^{2\pi} d\theta \int_0^\infty dk\, e^{k(z+\zeta)} \cdot \frac{\cos[k(x-\xi)\cos\theta]\cos(ky\sin\theta)}{k\cos^2\theta - g/U^2}$$

$$+ \frac{4g}{U^2} \int_0^{2\pi} d\theta \sec^2\theta\, e^{\frac{g}{U^2}(z+\zeta)\sec^2\theta} \sin\left[\frac{g}{U^2}(x-\xi)\sec\theta\right] \cdot \cos\left(\frac{g}{U^2} y \sin\theta \sec^2\theta\right) \tag{17}$$

where $\int$ means the principal-value integral.

Thus, from Equations (7) and (16), we get

$$\zeta_s(x,y) = \frac{U}{g} \phi_{sx}(x,y,0)$$

$$= -\frac{U^2}{2\pi g} \iint_{S^{(0)}} \frac{(x-\xi) f_\xi(\xi,\zeta)}{[(x-\xi)^2+y^2+\zeta^2]^{3/2}}\, d\xi d\zeta$$

$$- \frac{U^2}{2\pi g} \iint_{S^{(0)}} \hat{G}_{0x}(x-\xi,y,\zeta) f_\xi\, d\xi d\zeta \tag{18}$$

If we substitute the expression for $\hat{G}_{0x}(x-\xi,y,\zeta)$ from Equation (17) into Equation (18), we get

$$\zeta_s(x,y) = \frac{2}{\pi^2} \iint_{S^{(0)}} f_\xi(\xi,\zeta)\, d\xi d\zeta \int_0^{2\pi} d\theta \sec\theta$$

$$\cdot \int_0^\infty \frac{\sin[k(x-\xi)\cos\theta]}{k - \frac{g}{U^2}\sec^2\theta} \cos(ky\sin\theta) k e^{k\zeta} dk$$

$$- \frac{2g}{\pi U^2} \iint_{S^{(0)}} f_\xi\, d\xi d\zeta \int_0^{2\pi} d\theta \sec^3\theta\, e^{\frac{g}{U^2}\zeta\sec^2\theta}$$

$$\cdot \cos\left[\frac{g}{U^2}(x-\xi)\sec\theta\right] \cos\left(\frac{g}{U^2} y \sin^2\theta\sec^2\theta\right) \tag{19}$$

Within the first-order approximation, the wave profile along the side of the hull can be obtained by

$$\zeta_s(x,0) = \mathrm{Re}\left[-\frac{2i}{\pi^2} \iint_{S^{(0)}} f_\xi d\xi d\zeta \int_0^{2\pi} d\theta \sec\theta \cdot \int_0^\infty dk\, \frac{k e^{kZ'}}{k - k_0\sec^2\theta} - \frac{2g}{\pi U^2} \iint_{S^{(0)}} f_\xi d\xi d\zeta \cdot \int_0^{2\pi} d\theta \sec^3\theta\, e^{k_0\sec^2\theta Z'} \right] \tag{20}$$

where $k_0 = \frac{g}{U^2}$, $Z' = \zeta + i(x-\xi)\cos\theta$, and $i = \sqrt{-1}$, or

$$\zeta_s(x,0) = \mathrm{Re}\left[-\frac{2i}{\pi^2} \iint_{S^{(0)}} f_\xi d\xi d\zeta \cdot \left\{ \int_0^{2\pi} d\theta \sec\theta \int_0^\infty e^{kZ'} dk + k_0 \int_0^{2\pi} \sec^3\theta d\theta \int_0^\infty \frac{e^{kZ'}}{k - k_0\sec^2\theta}\, dk \right\} \right.$$

$$- \frac{2g}{\pi U^2} \iint_{S(\theta)} f_\xi d\xi d\zeta \int_0^{2\pi} d\theta \sec^3\theta \, e^{k_0 \sec^2\theta Z'} \Bigg] \qquad (21)$$

which amounts to the wave profile along the longitudinal centerplane.

Determination of Unsteady Free Surface

The free-surface deformation caused by the incident waves, diffracted waves, and motion-generated waves is obtained from Equations (4b) and (2). The unknown functions are ϕ_D, ϕ_k and $\bar{\zeta}_k$. In the following sections we describe procedures for obtaining these unknown quantities.

Diffraction Potential. From the kinematic boundary condition on the hull surface, we obtain from Equation (3)

$$\phi_{Dn}\Big|_{S_0} = -\phi_{In}\Big|_{S_0}$$

$$= K(jn_1\cos\mu + jn_2\sin\mu - n_3)\phi_I\Big|_{S_0} \qquad (22)$$

If we assume that the ship is slender such that $n_1 \ll n_2$, n_3, then, discarding n_1 in Equation (22), we obtain

$$\phi_{Dn}\Big|_{S_0} = K(jn_2\sin\mu - n_3)\phi_I$$

$$= j\omega\zeta_A(jn_2\sin\mu - n_3)$$

$$\cdot e^{-jK(x_0\cos\mu + y_0\sin\mu) + Kz_0} \qquad (23)$$

where (x_0, y_0, z_0) indicates a point on the hull surface S_0.

From Equation (23) we can infer that

$$\phi_D(x,y,z) \approx \phi(y,z;x)e^{-jKx\cos\mu} \qquad (24)$$

where x affects ϕ as a parameter rather than an independent variable. By applying the Laplacian operator to the right-hand side of Equation (24), we obtain

$$\phi_{yy} + \phi_{zz} - K^2\cos^2\mu\phi = 0 \qquad (25)$$

An appropriate linearized free-surface condition for the velocity potential $\phi(y,z;x)$ is

$$\left(j\omega_e - U\frac{\partial}{\partial x}\right)^2 \phi(y,0;x)e^{-jKx\cos\mu}$$

$$+ g\phi_z e^{-jKx\cos\mu} = 0 \qquad (26)$$

or using the relation $\omega_e = \omega - KU\cos\mu$, we have

$$\phi_z(y,0;x) - K\phi = 0 \qquad (27)$$

The kinematic body-boundary condition for ϕ is

$$\phi_N\Big|_{C_0(x)} = j\omega\zeta_A(jN_2\sin\mu - N_3)$$

$$\cdot e^{-jKy_0\sin\mu + Kz_0} \qquad (28)$$

where $\underline{N} = (N_2, N_3)$ is the two-dimensional unit vector on $C_0(x)$ which is the immersed contour of a cross section at x. The far field condition as $|y| \to \infty$ is given as[7]

$$\phi \sim \begin{cases} e^{jK|y|\sin\mu} & \text{for } \mu \neq \pi \\ |y| & \text{for } \mu = \pi \end{cases} \qquad (29)$$

In fact, we find that the boundary-value problem for ϕ is confined in the y-z plane; hence, if we find an appropriate Green's function, G, which satisfies Equations (25), (27) and (29), we can obtain the solution in the form of

$$\phi(y,z;x) = \int_{C_0(x)} Q(l)G(l;y,z)dl \qquad (30)$$

where the unknown function Q should be found from the remaining boundary condition (28). The appropriate Green's function was given by Ursell,[6] and the solution for ϕ was obtained by Choo[7] and Troesch.[8]

The approximation of ϕ_D by Equation (24), where the variable x is suppressed as a parameter, has led to the free surface condition (27) and the far-field condition (29). As one can readily observe, the forward-speed effect is nonexistent in the foregoing problem. The foregoing simplification can be criticized for the lack of consistency in the perturbation scheme. However, the analysis will be pursued on this basis with the assumption that the forward speed has no significant effect on the wave diffraction. Furthermore, under the assumption that the wave lengths of interest are greater than the order of ship beam, the Helmholz equation given by (25) will be replaced by the Laplace Equation, i.e.,

$$\phi_{yy} + \phi_{zz} = 0 \qquad (31)$$

which is exact for $\mu = \pi/2$, i.e., beam waves. A further digression from the original problem will be made with a heuristic argument, based on the success of strip theory, that the near-field solution derived with the radiation condition

$$\lim_{y \to \pm\infty} (\phi_y \mp jK\phi) = 0 \qquad (32)$$

is acceptable.*

*Although the diffraction potential is not explicitly solved in the usual ship motion theory based on the strip assumption, a similar radiation condition is invoked in applying the Haskind relation in the two dimensional sense.

Thus, the modified boundary-value problem now is reduced to an almost identical problem of forced oscillation of two-dimensional cylinders in a free surface in the combined modes of heave and sway. It should be noted that the diffraction potential is a function of the wave frequency ω. This is a noticeable difference from the strip solution used in the ship motion computation[4] in which the diffraction potential is treated as a function of wave-encounter frequency ω_e. In Appendix I, the process of solving the diffraction potential satisfying the two-dimensional Laplace Equation (31) with the boundary conditions (27), (28) and (32) is described. The description is given in a general form for any prescribed function replacing the right-hand side of Equation (28).

Motion and Radiation Potential. The motion of the ship is obtained by solving two sets of linearized coupled equations of motion, which, according to the coordinate system given in Figure 1, for k,ℓ = 1, 3, 5 and k,ℓ = 2, 4, 6, are

$$\sum_{\ell} (M_{k\ell} + A_{k\ell})\ddot{\xi}_\ell + B_{k\ell}\dot{\xi}_\ell + C_{k\ell}\xi_\ell = F_k^{(e)} \quad (33)$$

Here,

$$M_{k\ell} = \begin{cases} M(\text{mass of ship}) & \text{for } k=\ell \le 3 \\ I_{kk}(\text{mass moment of inertia}) & \text{for } k=\ell \ge 4 \\ 0 & \text{for } k\neq\ell \text{ except for } M_{24} = M_{42} = -z_g M \text{ where } z_g \text{ is the vertical coordinate of the center of gravity;} \end{cases}$$

$A_{k\ell}$ is the added mass coefficient in the kth mode due to the motion in the ℓth mode; $B_{k\ell}$ the corresponding damping coefficient; $C_{k\ell}$ the restoring coefficient; and $F_k^{(e)}$ the wave excited force or moment.

The coefficients in the equations of motion are obtained by slender-body strip theory.[4] The expressions are given as follows:

$$A_{k\ell} = \mathrm{Re}_j \left[-\frac{\rho}{\omega_e^2} \int_L dx \int_{C(x)} (\phi'_{kN}(y,z;x) - 2UN_3\delta_{k5} + 2UN_2\delta_{k6})\phi'_\ell \, dl \right] \quad (34)$$

$$B_{k\ell} = \mathrm{Im}_j \left[-\frac{\rho}{\omega_e} \int_L dx \int_{C(x)} (\phi'_{kN} - 2UN_3\delta_{k5} + 2UN_2\delta_{k6})\phi'_\ell \, dl \right] \quad (35)$$

for k,ℓ = 1, 2, . . . , 6.

where Re_j and Im_j are the real and imaginary parts, respectively, of a complex function, the imaginary part of which is preceded by $j = \sqrt{-1}$; $\int_L dx$ is the integral over the length in the positive x direction and $\int_{C(x)} dl$ the integral over the submerged contour of the cross section located at x; ϕ'_k is the two-dimensional approximation of ϕ_k; and $\delta_{k\ell}$ is the Kronecker delta.

The restoring coefficients $C_{k\ell}$ are given by $C_{33} = \rho g \forall$, $C_{24} = -\rho g \forall$, $C_{35} = \rho g A_w$, $C_{53} = \rho g M_w$, $C_{44} = \rho g \forall (I_{xx}/\forall - \overline{OB})$, and $C_{55} = \rho g \forall (I_{yy}/\forall - \overline{OB})$ where $\forall$ is the displaced volume, A_w the waterplane area, M_w the moment of the waterplane area about the y-axis, I_{xx} and I_{yy}, respectively, the mass moment of inertia about the x- and y-axis, and $\overline{OB}$ the vertical distance from the center of buoyancy to the calm waterline. The wave excited forces are given by

$$F_k^{(e)} = \rho \int_L dx \int_{C(x)} \left[-j\omega N_k + \frac{\omega}{\omega_e} \left\{ \phi'_k(y,z;x) + \frac{U}{j\omega_e}\phi'_2\delta_{k5} - \frac{U}{j\omega_e}\phi'_3\delta_{k5} \right\} \frac{\partial}{\partial N} \right] \phi_I \, dl \quad (36)$$

for k = 1, 2, . . . , 6, where $N_4 = yN_3 - zN_2$, $N_5 = -xN_3$ and $N_6 = xN_2$.

From the foregoing equations it is obvious that if the motion potentials $\phi'_k(y,z;x)$ are known, we can solve the equations of motion and find the six-degrees of freedom motion ξ_k. The first three of ξ_k are the linear displacements from the mean position of the ship in the x, y, and z directions, respectively, and the remaining three are the angular displacements about the x, y, and z axes, respectively. In numerical order of k these are called surge, sway, heave, roll, pitch and yaw motion. Utilizing the derivation shown in Appendix I, we can show that

$$\begin{aligned} \phi_0(x,y,z) &= \phi_I + \phi_D(y,z;x) + \sum_{k=1}^{6} \phi'_k(y,z;x)\bar{\xi}_k \\ &= \phi_I + \phi_D + \phi'_1\bar{\xi}_1 + \phi'_2\bar{\xi}_2 + \phi'_3\bar{\xi}_3 + \phi'_4\bar{\xi}_4 \\ &\quad - \left(x + \frac{jU}{\omega_e}\right)\phi'_3\bar{\xi}_5 + \left(x + \frac{jU}{\omega_e}\right)\phi'_2\bar{\xi}_6 \end{aligned} \quad (37)$$

Substitution of Equation (37) into Equation (4b) yields

$$\begin{aligned} \zeta_0(x,y) &= -\frac{j\omega}{g}(\phi_I(x,y,0) + \phi_D) \\ &\quad + \frac{2U}{g}(\phi'_2\bar{\xi}_6 - \phi'_3\bar{\xi}_5) - \frac{j\omega_e}{g}[\phi'_1\bar{\xi}_1 + \phi'_2(\bar{\xi}_2 + x\bar{\xi}_6) \\ &\quad + \phi'_3(\bar{\xi}_3 - x\bar{\xi}_5)] \end{aligned} \quad (38)$$

III. Numerical Checks

For the purpose of illustrating computations, a pontoon having uniform cross sections of the midship of a Mariner Class ship is chosen. The length of the pontoon is arbitrarily taken as five times the beam. The cross section is close to a rectangle except for the rounded bilges. The immersed dimension of the cross section is 23.06 m beam and 9.07 m draft. The offsets used to describe the section are given in Table 1 and the section view is given in Figure 2.

Table 1 — Offsets of Right-Half of Midship Section of Mariner Class Ship

Y (m)	Z (m)
0.	-9.088
4.353	-9.088
8.705	-9.088
10.380	-8.458
10.958	-7.849
11.480	-6.629
11.534	-4.191
11.53	0.

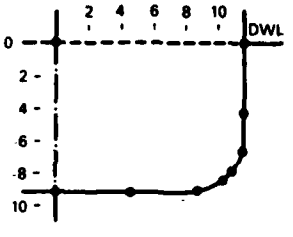

Figure 2 — Right-Half Cross Section View of Midship of Mariner Class Ship

As described in Appendix I, the velocity potentials are obtained by using the method of source distribution on the immersed contour of the cross section of the body. As shown by Equation (I-7), an approximation is made by assuming a constant source strength on each line segment which makes up the contour. The line segments are made by connecting the adjacent two points on the contour by a straight line. The points chosen are as shown in Figure 2. It can be expected that numerical accuracy will increase as the number of points chosen on the contour increases; however, a compromise should be made to minimize computer costs. A total of eight boundary points are taken on the right half of the immersed contour of a cross section as shown by the black dots in Figure 2. The boundary points thus chosen provided the desired accuracy and yielded a satisfactory numerical convergence.

It is well known that the method of Green's function to solve for the velocity potential associated with an oscillating body in a free surface suffers from the existence of indefinite solutions at certain frequencies.[9] Descriptions of the existence of the indefinite solutions and their removal are given in Appendix II. To remove the indefinite solutions, the source distribution is extended on the line z = 0 inside the body, and a rigid wall condition, $\phi'_z = 0$, is imposed on that line, which will be referred to as "top deck" hereafter. According to Frank[10] the "irregular frequencies" for a rectangle of beam B and draft T are obtained by

$$K_m b = \omega_m^2 b/g = \frac{m\pi}{2} \coth(m\pi T/B), \quad m = 1, 2, 3, \ldots$$

where $b = \frac{B}{2}$. For the section considered here, B/T = 2.54, and therefore we get $K_1 b = 1.86$, and $K_2 b = 3.19$. In Figure 3, the singular behavior of the amplitude of the free surface motion due to beam regular waves at y = 1.05b (the wave incident side) at the first irregular frequency is shown. The amplitude of the wave is normalized by the incident-wave amplitude, i.e., $|\zeta_0|/\zeta_A$ where ζ_0 is obtained by Equation (38). The solid line is obtained by taking two line segments on the top deck between y = 0 and y = b, and y = 0 and y = -b, and imposing the condition $\phi_z = 0$. In Table 2, a comparison of the free-surface amplitudes is presented for various top-deck conditions. The values for the rigid-wall conditions imposed on up to six line segments on the top deck are given together with that obtained by imposing the $\phi' = 0$ condition on the two line segments on the top deck. Also shown are the values obtained by $\phi'_z = 4$ on the two line segments on the top deck at Kb = 0.3, 1.0 and 2.0. The latter values are shown to check Ohmatsu's statement[11] that any arbitrary values for ϕ'_z on the top deck, provided an appropriate symmetric or anti-symmetric condition is maintained, can be chosen to remove the irregular frequencies. It appears that the method holds in higher frequencies only in the present case. It looks obvious from Equation (II-6) that, unless $\phi'_z = 0$ or $\phi' = 0$ is imposed on the top deck, there is no guarantee that the trivial solution for ϕ' in the interior domain will be obtained. One would assume that more segments on the top deck should yield better results; however, the values obtained near Kb = 1.0 for 4 and 6 segments on the top deck show that the assumption is not necessarily true. Why more than two segments on the top deck show an irregular behavior in the vicinity of Kb = 1.0 is not yet clear. Based on this investigation, the two segments on the top deck, together with the other segments on the body contour, are chosen for the ensuing computations.

Table 2 – Free-Surface Amplitudes at y = 1.05b for Various Top-Deck Conditions

Kb	No Top	2 Seg.	$\phi_{z=0}$ 4	6	ϕ = 0 2 Seg.	ϕ_z = 4 2 Seg.
0.3	0.932	0.932	0.932	0.933	0.926	0.842
0.8	1.483	1.428	1.389	1.360	1.510	
0.9	1.528	1.470	1.381	1.366	1.508	
1.0	1.212	1.168	0.880	0.706	1.247	0.948
1.1	1.313	1.271	2.662	3.034	1.324	
1.2	1.946	1.877	2.367	2.427	1.838	
1.6	2.143	1.992	2.010	2.009	2.003	
1.65	2.156	1.985	1.989	1.986	1.996	
1.70	2.179	1.977	1.970	1.964	1.989	
1.75	2.228	1.970	1.953	1.944	1.982	
1.80	2.356	1.962	1.937	1.926	1.975	
1.85	3.386	1.955	1.922	1.909	1.968	
1.90	1.231	1.948	1.909	1.894	1.961	
1.95	1.734	1.941	1.897	1.880	1.954	
2.0	1.843	1.935	1.887	1.868	1.947	1.937
2.5	1.966	1.877	1.853	1.830	1.883	

Table 3 – Comparison of Wave Excited Forces Obtained by Eq. (36) and Eq. (39)

Kb	$\lvert F_2^{(e)} \rvert / A$		$\lvert F_3^{(e)} \rvert / A$		$\lvert F_4^{(e)} \rvert / A$	
	(36)	(39)	(36)	(39)	(36)	(39)
0.1	0.1525	0.1536	0.8121	0.8175	0.0062	0.0062
0.5	0.5861	0.5888	0.5116	0.5161	0.0502	0.0500
0.9	0.5718	0.5761	0.3429	0.3449	0.0670	0.0668
1.4	0.4696	0.4776	0.2177	0.2101	0.0690	0.0692
2.0	0.3780	0.3903	0.1089	0.1104	0.0642	0.0654

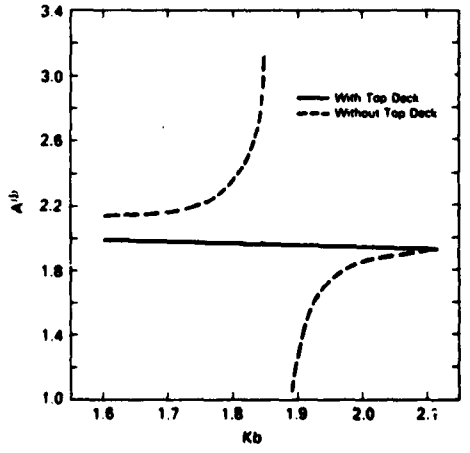

Figure 3 – Removal of Singular Behavior at Irregular Frequency

Several cross checks of the numerical results were made to ensure the accuracy of the computations. One was a correlation of the wave-excited forces computed by two independent methods; one by a direct computation using the expression given by Equation (36) and the other by an indirect method using the damping coefficients. The latter method is given by Newman[12] as

$$\left|F_k^{(e)}\right| / \zeta_A = (\rho g^2 B_{kk}/\omega)^{\frac{1}{2}} \qquad (39)$$

for two-dimensional bodies for μ = 90 degrees. The comparison of the two independent results given in Table 3 shows a good agreement which gradually deteriorates up to about 3 percent difference at Kb = 2. In any case a 3 percent difference is well within the numerical errors resulting from the segmentation of the boundary contour of a cross section. The denominator A in Table 3 equals to $2\rho g b \zeta_A$ for $|F_2^{(e)}|$ and $|F_3^{(e)}|$ and $2\rho g b^2 \zeta_A$ for $|F_4^{(e)}|$.

The hydrodynamic coefficients resulting from the coupling between the sway and roll modes are A_{24}, A_{42}, B_{24}, and B_{42}. From Green's theorem we have

$$\iint_S (\phi_k \phi_{\ell n} - \phi_\ell \phi_{kn}) ds = 0 \qquad (40)$$

where S is the surface bounding the fluid domain which consists of the body surface S_B, the free surface S_F, and a vertical cylinder surface S_R of a large radius R with a bottom closure S_B. Since $\phi_{kn} = \phi_{kz} = K\phi_k$ on S_F, $\phi_{kz} = 0$ on S_B, and $\phi_k = 0(1/\sqrt{R})$ on S_R, we can show that

$$\iint_{S_B} \phi_k \phi_{\ell n} ds = \iint_{S_B} \phi_\ell \phi_{kn} ds$$

which means that

$$A_{2\ell} = A_{\ell 2} \quad \text{and} \quad B_{2\ell} = B_{\ell 2}$$

from Equations (34) and (35). The values of these coefficients are shown in Table 4. Although the percent difference between the two values at the higher frequencies appears large, the error is within the bound which is associated with the number of segments chosen in the present case.

Table 4 – Comparison of Coupled Sway-Roll ($\bar{A}_{24}$ and $\bar{B}_{24}$) and Roll-Sway ($\bar{A}_{42}$ and $\bar{B}_{42}$) Coefficients

Kb	$\bar{A}_{24}$	$\bar{A}_{42}$	$\bar{B}_{24}$	$\bar{B}_{42}$
0.3	0.1272	0.1245	0.0334	0.0316
1.0	0.0503	0.0514	0.0865	0.0866
2.0	0.0068	0.0085	0.0867	0.0882

The expression for a pulsating source of unit strength below a free surface is given by Equation (I-5). The principal-value integral in this equation can be converted to an exponential integral in the form

$$\int_0^\infty \frac{e^{k(z+\zeta)}\cos k(y-\eta)}{\alpha - k} dk$$

$$= \mathrm{Re}\left[-e^{-i\alpha S} E_1(-i\alpha S) \pm i\pi e^{-i\alpha S}\right];$$

the plus sign for $y-\eta > 0$ and the minus sign for $y-\eta < 0$

where

$$S = (y-\eta) + i(z+\zeta)$$

$$E_1(S) = \int_S^\infty \frac{e^{-t}}{t} dt$$

$$= \gamma + \ln S + \sum_{n=1}^{\infty} \frac{(-1)^n S^n}{n\,n!}, \quad |\arg S| < \pi,$$

$\gamma = 0.57721566\ldots$ = Euler's constant.

For the evaluation of $E_1(S)$, one can use the above equation; however, when $|S|$ is large, the infinite series makes the computation inefficient. Thus, one can use various rational and polynomial approximations for a large argument.[13] In this work the Laguerre quadrature method introduced by Todd[14] is used.

To obtain the free surface elevation $r_0(x,y)$ the velocity potentials should be evaluated at $z = 0$, which in turn means that the Green's function given by Equation (I-5) should be evaluated at $z = 0$. Then, for the sources at the top deck, the principal-value integral becomes

$$\int_0^\infty \frac{\cos k(y-\eta) - i\sin k(y-\eta)}{\alpha - k} dk$$

$$= \cos\alpha X\, Ci(\alpha X) + \sin\alpha X \left|\frac{\pi}{2} + Si(\alpha X)\right|$$

$$- i\left|\sin\alpha X\, Ci(\alpha X) - \cos\alpha X \left\{\frac{\pi}{2} + Si(\alpha X)\right\}\right|$$

where $X = y-\eta$, and Si and Ci are the sine and cosine integrals, respectively, which are given by

$$Si(x) = \frac{\pi}{2} - \int_x^\infty \frac{\sin t}{t} dt = \sum_{n=0}^{\infty} \frac{(-1)^n x^{2n+1}}{(2n+1)(2n+1)!}$$

$$Ci(x) = -\int_x^\infty \frac{\cos t}{t} dt = \gamma + \ln x + \sum_{n=1}^{\infty} \frac{(-1)^n x^{2n}}{2n(2n)!}$$

Since these two functions approach zero in an oscillatory manner as $x \to \infty$, the series computation for large x is expected to require a large number of terms before converging to the desired accuracy (error less than 10^{-7}). The rational approximation of Hastings[15] (see, e.g., p. 233 of Reference 13) was employed to obtain the sine and cosine integrals, and the results were found to be identical to those of the Laguerre method of Todd.[14]

The amplitude of the radiating waves at $y = 100b$ generated by the sway and heave motion of unit amplitude are given in Table 5. The values given under the heading "Infinity" are obtained in terms of the damping, B_{ij}, by

$$\bar{A}^{(i)} = \frac{\omega}{g}(B_{ij}/\rho)^{\frac{1}{2}}, \quad i = 2, 3$$

which can be obtained from the principle of energy conservation and are exact at $y = \infty$. It appears that the radiating wave generated by sway motion yields better accuracy than that generated by heave motion.

Table 5 — Comparison of Radiating-Wave Amplitudes Due to Motion at $y = 100b$

Kb	$\bar{X}^{(3)}$		$\bar{X}^{(5)}$	
	Todd	∞	Todd	∞
0.3	0.289	0.297	0.389	0.391
1.0	1.111	1.100	0.613	0.625
2.0	1.589	1.570	0.380	0.430

IV. Results and Discussion

The sample computation is performed for the condition of zero speed, i.e., $U = 0$. Thus, there is no contribution from the steady translation to the free-surface elevation which is given by Equation (19).

To obtain the relative motion, the absolute vertical motion of the body should be known. In Figures 4 through 6, the motion amplitudes per unit incident-wave amplitude are shown versus the nondimensional frequencies $\omega^2 b/g = 2\pi b/\lambda$ for $\mu = 90$, 135 and 180 degrees. Due to the symmetry of the body, there is no motion at $\mu = \pi$ (head waves) for sway and roll. To facilitate the understanding of the measure of the vertical displacement at the beam end which is contributed by roll, the roll amplitude is multiplied by the half beam b in Figure 6.

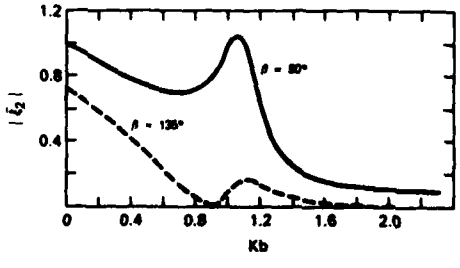

Figure 4 — Sway Amplitude at Zero Speed for Various Wave Headings

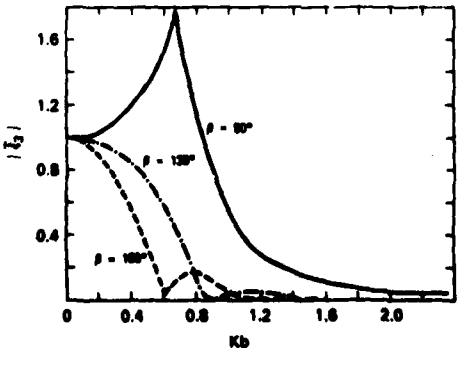

Figure 5 — Heave Amplitudes at Zero Speed for Various Wave Headings

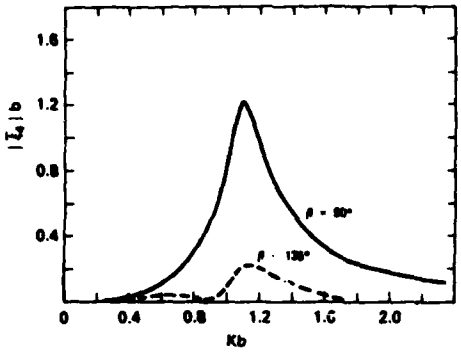

Figure 6 — Roll Amplitudes at Zero Speed for Various Wave Headings

Since the pontoon is symmetric fore and aft, the equations of motion given by Equation (33) (neglecting the surge motion and its coupling effects) can be reduced to the following form:

$$(M + A_{33})\ddot{\xi}_3 + B_{33}\dot{\xi}_3 + C_{33}\xi_3 = F_3^{(e)}$$

$$(M + A_{22})\ddot{\xi}_2 + B_{22}\dot{\xi}_2 + (A_{24} - Mz_0)\ddot{\xi}_4 + B_{24}\dot{\xi}_4 + C_{24}\xi_4 = F_2^{(e)} \qquad (41)$$

$$(A_{42} - Mz_0)\ddot{\xi}_2 + B_{42}\dot{\xi}_2 + (I_{44} + A_{44})\ddot{\xi}_4 + B_{44}\dot{\xi}_4 + C_{44}\xi_4 = F_4^{(e)}$$

The coefficients appearing in Equation (41) are obtained from Equations (34) and (35) in terms of the two-dimensional velocity potential $\phi'(y,z;x)$. The z-coordinate of the center of gravity, z_0, was approximated as that of the center of buoyancy. The radius of gyration for roll was assumed to be 0.6b such that $I_{yy} = M(0.6b)^2$.

It is well known that a prediction of roll motion based on linear damping obtained by a velocity potential at zero speed would yield an over-predicted peak roll at its resonant frequency. An iterative scheme to obtain a convergence of roll motion using the equivalent linear damping of the viscous damping could have been tried in order to suppress the peak roll; however, to avoid the ambiguity resulting from the approximation of the viscous damping, it was decided not to employ this scheme.

The strip method employed for the computation of motion does not take into account the end effects of the pontoon. Thus, the lengthwise integrals in evaluating the $A_{k\ell}$ and $B_{k\ell}$ become simple integrals such as

$$\int_L \alpha_{k\ell}\, dx = \alpha_{k\ell} L$$

or

$$\int_L \alpha_{k\ell} x^2\, dx = \alpha_{k\ell} L^3/12$$

where $\alpha_{k\ell}$ is the sectional quantity of $A_{k\ell}$ or $B_{k\ell}$. Similarly, for the wave excited forces $F_k^{(e)}$, the contribution from the lengthwise integral becomes

$$\int_{-\frac{L}{2}}^{\frac{L}{2}} e^{jKx\cos\mu}\, dx = \frac{2\sin\left(\frac{KL}{2}\cos\mu\right)}{K\cos\mu} \qquad (42a)$$

or

$$\int_{-\frac{L}{2}}^{\frac{L}{2}} x e^{jKx\cos\mu}\, dx = j\left[\frac{2\sin\left(\frac{KL}{2}\cos\mu\right)}{K^2\cos^2\mu} - \frac{L\cos\left(\frac{KL}{2}\cos\mu\right)}{K\cos\mu}\right] \text{ for } \mu \neq \frac{\pi}{2} \qquad (42b)$$

$$= 0 \quad \text{for } \mu = \frac{\pi}{2}$$

For the arbitrary pontoon geometry chosen in the present sample calculation, the pitch and yaw motions for $\mu \neq \pi/2$ do not bear much significance because they are functions of the length of the body which is arbitrarily chosen in the present case. Thus, the results to be illustrated will be limited to beam waves, i.e., $\mu = \pi/2$, only. However, the motion amplitudes in Figures 4 to 6 for $\mu \neq \pi/2$ are presented to show that for a body which is symmetric fore and aft as well as port and starboard, beam waves could produce larger relative motion than the other wave headings. It is of interest to note in Figure 5 that the heave amplitude is less than the incident wave amplitude at all wave lengths for both $\mu = 135$ and 180 degrees. This fact seems to reflect the behavior of the function given by Equation (42b) which is the lengthwise contribution of the heave exciting force. One can readily see that the function sin x/x where $x = \cos\mu\, KL/2$ has the maximum value of unity at $x = 0$ and monotonically decreases as x increases. Thus, as either the absolute value of $\cos\mu$ or K increases, the wave excited heave force decreases. The sway motion contributes to the relative motion through its wavemaking which changes the free-surface elevation at the ship sides.

The local waves generated by the sway, heave, and roll motion are presented in Figure 7 as $\bar{A}_2$, $\bar{A}_3$, and $\bar{A}_4$, respectively, where the bar indicates that the quantities are nondimensionalized by incident wave amplitude. The beamwise location of these free-surface amplitudes is 1.05b from the origin. As can be observed in the figure the maximum local wave amplitudes occur at the same frequencies at which the respective motion amplitude becomes maximum. The trend of the curves shown in Figure 7 is found to be almost independent of the beamwise locations, although the magnitudes can change significantly. For the body chosen in the present case, the sway motion appears to be a better wavemaker than the heave motion per unit amplitude of the incident wave from the beam directions for higher frequencies, i.e., $Kb > 0.8$.

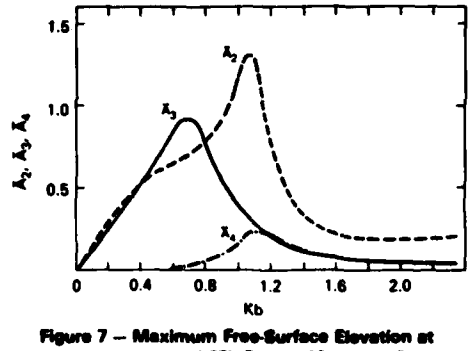

Figure 7 — Maximum Free-Surface Elevation at $y = \pm 1.05b$ Due to Motion in Sway ($\bar{A}_2$), Heave ($\bar{A}_3$) and Roll ($\bar{A}_4$)

Combination of these motion-generated waves will be a harmonically oscillating free surface. The amplitude of this free-surface oscillation at $y = \pm 1.05b$ is shown in Figure 8 as $\bar{A}_H$ which is a nondimensional quantity normalized by the incident wave amplitude. The free surface deformation due to the incident and diffracted waves should be added to the motion-generated free-surface disturbance to obtain the actual free-surface elevation at the sides of a ship. The diffracted waves are the reflected and the transmitted waves. At the incident side of the body, the free surface deformation is caused by the combination of the incident and reflected waves. The amplitude of the combined waves of incidence and reflection at the incident side at $y = 1.05b$ is indicated by $\bar{A}_H^{(I)}$ in Figure 8. The transmitted wave amplitude at the lee side at $y = -1.05b$ is indicated by $\bar{A}_H^{(L)}$. The bar sign indicates a nondimensionalization by the incident wave amplitude. As one can observe from Figure 8, the free surface oscillates near the body at the incident side with twice the amplitude of the incident wave for $Kb > 0.6$, i.e., the incident wave length less than about 10b. On the other hand, at the lee side the free surface fluctuates with less than about 40 percent of the incident wave amplitudes for $Kb > 0.6$.

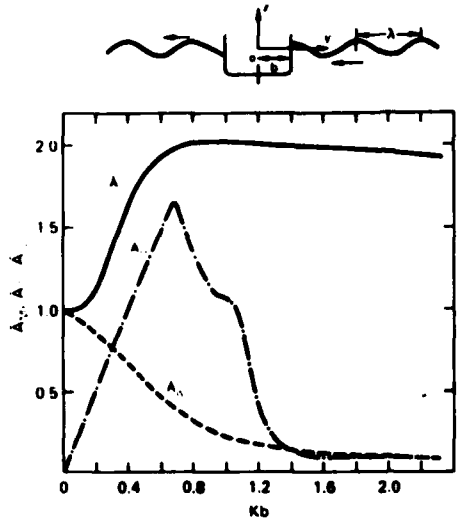

Figure 8 — Maximum Free-Surface Elevation at $y = \pm 1.05b$ Due to Motion ($\bar{A}_M$) and Diffraction ($\bar{A}_W^{(R)}$, $\bar{A}_W^{(L)}$) for Beam Waves

By the principle of the conservation of energy the following relation should hold

$$\left(\bar{A}_W^{(R)}\right)^2_{y=\infty} + \left(\bar{A}_W^{(T)}\right)^2_{y=-\infty} = 1$$

where $\bar{A}_W^{(R)}$ and $\bar{A}_W^{(T)}$ are, respectively, the amplitude ratios of the reflected and transmitted waves to the incident waves. A check was made at $|y| = 100b$ to confirm the foregoing relation. It was found that the relation holds true even at distances as short as 100b. However, when the distribution of the source is extended onto the waterline inside of the body, the square sum of the foregoing equation becomes slightly less than unity. This is construed as an indication that the added top deck may introduce a slightly greater numerical error than the case without the top deck. It is uncertain if $\bar{A}_W^{(I)}$ can be greater than 2 even at values of y as small as 1.05b. Although no firm proof is established, it appears that the values of $\bar{A}_W^{(I)}$ exceeding 2 are due to numerical errors resulting from the segment approximation.

The amplitudes of the free surface motion generated by the body motion and the incident and diffracted waves are shown in Figure 9 at the incident and the lee sides of the body. The prominent hump and hollow trend of the amplitude curves indicates the sensitivity of the free surface movement with respect to the incident wave frequency. The drastic change from the behavior of individual wave amplitudes shown in Figure 8 implies that the phase differences between the motion-generated waves and the diffracted waves can vary from 0 degree to ±180 degrees.

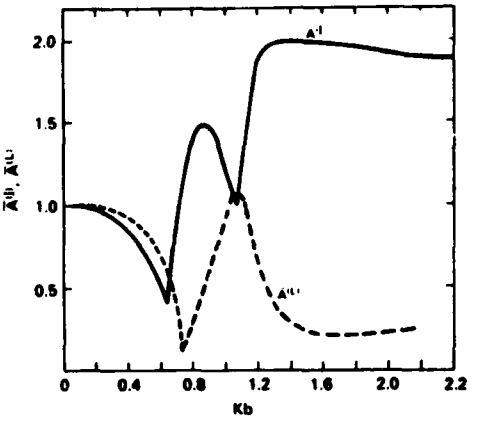

Figure 9 — Maximum Free-Surface Elevation at $y = \pm 1.05b$ Due to the Combined Effects of Motion and Diffraction for Beam Waves

To show the behavior of the amplitudes of the waves as a function of y, the motion-generated wave and the reflected wave at $Kb = 0.8$ are chosen and are presented in Figure 10. The values shown are those normalized by ζ_A. The solid curve is for the motion-generated wave, and the dotted one is for the reflected wave. A larger scale for y/b is taken near the hull to examine the behavior more closely. For $Kb = 0.8$ the wave length (λ) is 7.85b. One can observe at about $y = 12b \approx 1.5\lambda$ that the outgoing-wave amplitudes become identical to the far-field values. The local waves appear to be confined within one-beam distance from the hull. Generally, this trend is confirmed at other frequencies. However, when all the waves are superposed with their proper phases, the amplitude behavior becomes much more radical as shown by the chained curve in Figure 10. The sharpness of the curve is indicative of a possibility of breaking waves somewhere between y = 1.5b and 4.0b.

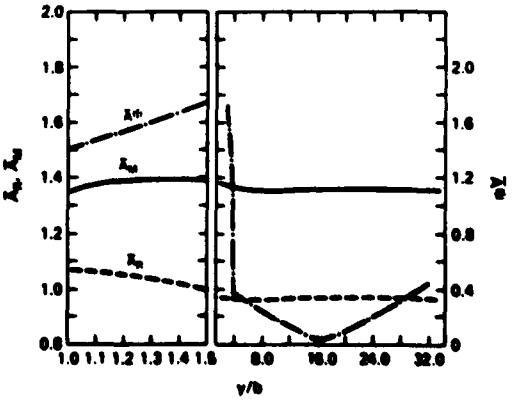

Figure 10 — Amplitude of Waves by Motion ($\bar{A}_M$) and Reflection ($\bar{A}_W$) at Kb = 0.8

The amplitudes of the absolute ($|\bar{\zeta}_v|$) and the relative ($|\bar{\zeta}_R|$) motion divided by the incident wave amplitude are shown in Figure 11 for y = 1.05b and in Figure 12 for y = -1.05b. The relative motion computed on the basis of no deformation of the incident wave is designated as "Old Rel." and the present calculation based on the deformation of the incident waves is designated as "New Rel.". A large difference between the old and new relative motion can be observed in Figure 11 at higher frequencies. The difference is almost a factor of two. This phenomenon is due to the fact that at higher frequencies the absolute vertical motion of the body diminishes while the reflection effect almost doubles the amplitude of the free surface motion on the side of the body. The old relative motion, however, assumes that there is no deformation of the incident wave; hence, the relative-motion amplitude becomes identical to the incident-wave amplitude. On the other hand, the new relative motion at the lee side diminishes at higher frequencies since both the absolute motion and transmitted wave amplitudes diminish, while the old relative motion amplitude becomes the same as the incident wave amplitude.

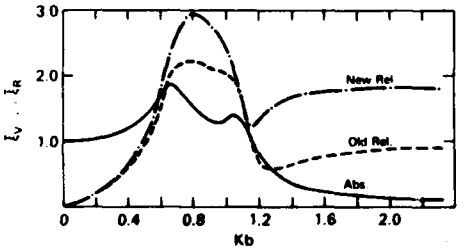

Figure 11 – Relative Motion and Absolute Motion at y = 1.05b for Beam Waves

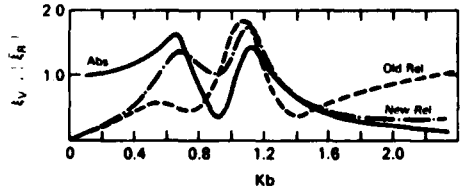

Figure 12 – Relative Motion and Absolute Motion at y = -1.05b for Beam Waves

V. Conclusion

From the present investigation it is found that neglecting the incident-wave deformation due to the body motion and diffraction could lead to a significant error in the prediction of the relative motion of ships. The computation should be extended to an actual ship at speed for various wave headings, and the results should be correlated with available model experimental results of relative motion.

VI. Acknowledgments

This study was sponsored by the Naval Sea Systems Command under the General Hydromechanics Program administered by the David Taylor Naval Ship R&D Center. Thanks are extended to Mr. V. J. Monacella and Dr. W. C. Lin for their kind support during the course of this work.

Appendix I

Determination of the Velocity Potentials $\phi_D'(y,z)$ and $\phi_k'(y,z)$

The boundary condition to be satisfied by the harmonic functions $\phi_D'(y,z)$ and $\phi_k'(y,z)$ are as follows:

$$\phi_z' - \alpha\phi' = 0 \quad \text{on } z = 0 \tag{I-1}$$

where $\alpha = \omega^2/g$ for ϕ_D' and $\alpha = \omega_e^2/g$ for ϕ';

$$\phi_N'\big|_{C_0} = f \tag{I-2}$$

where C_0 is the contour below the calm water surface of a cross section of a ship and f, a complex function, is assumed to be known;

$$\lim_{y \to \pm\infty} (\phi_y' \mp j\alpha\phi') = 0 \tag{I-3}$$

and

$$\phi_z' = 0 \quad \text{as } z \to -\infty. \tag{I-4}$$

The Green's function $G(y,z;\eta,\zeta)$ which is in the form

$$G = \ell n\, r + H(y,z;\eta,\zeta)$$

where

$$r = [(y-\eta)^2 + (z-\zeta)^2]^{\frac{1}{2}}$$

and

$$\left(\frac{\partial^2}{\partial y^2} + \frac{\partial^2}{\partial z^2}\right) H = 0$$

in $z \leq 0$, is given in Wehausen and Laitone[5] as

$$G = \frac{1}{2\pi}\left[\ell n\, r - \ell n\, r' - 2\int_0^\infty \frac{e^{k(z+\zeta)}\cos k(y-\eta)}{k-\alpha}\, dk + j2\pi e^{\alpha(z+\zeta)}\cos\alpha(y-\eta)\right] \tag{I-5}$$

where $r' = [(y-\eta)^2 + (z+\zeta)^2]^{\frac{1}{2}}$. Using this Green's function, we can express ϕ' by

$$\phi'(y,z) = \int_{C_0} Q(l)G(l;y,z)\,dl \tag{I-6}$$

where Q is the unknown to be determined. Since G represents a pulsating source at a point below the calm water surface, Q can be regarded as an unknown source strength of complex value.

Following the procedure adopted by Frank,[10] we can show that

$$\phi'(y,z) \approx \sum_{j=1}^{N} Q_j \int_{C_j} G(l;y,z)dl \qquad (I\text{-}7)$$

where C_0 is divided into N even number of linear segments C_j, and Q_j is the constant source strength on the jth line segment C_j.

Let us assume that the prescribed function f can be [illegible] to an even function, $f^{(e)}$, and an odd [illegible] $f^{(o)}$, of y. The cross section [illegible] is assumed to be symmetric about the z-axis. Thus, we can also assume [illegible] that ϕ' can be divided into an even part ($\phi^{(e)}$) and an odd part $\phi^{(o)}$. Then, we can [illegible] that:

$$\phi^{(e)} \approx \sum_{j=1}^{M} Q_j^{(e)} \int_{C_j} G^{(e)}(l;y,z)dl \qquad (I\text{-}8)$$

$$\phi^{(o)} \approx \sum_{j=1}^{M} Q_j^{(o)} \int_{C_j} G^{(o)}dl \qquad (I\text{-}9)$$

where M = N/2 is the number of linear segments on the right-half of C_0, and

$$\left.\begin{matrix} G^{(e)} \\ G^{(o)} \end{matrix}\right\} = \frac{1}{2\pi}\left[\ln r \pm \ln r_1 - \ln r' \mp \ln r_1' \mp 2\int_0^{\infty} \frac{e^{k(z+\zeta)}\cos k(y\mp\eta)}{k-\alpha}\,dk \pm j2\pi e^{\alpha(z+\zeta)}\cos\alpha(y\mp\eta)\right] \qquad (I\text{-}10)$$

where the upper and lower signs correspond respectively to $G^{(e)}$ and $G^{(o)}$, and

$$r_1 = [(y+\eta)^2 + (z-\zeta)^2]^{\frac{1}{2}},$$

$$r_1' = [(y+\eta)^2 + (z+\zeta)^2]^{\frac{1}{2}}.$$

Now, if we take the normal derivative of $\phi^{(e)}$ and $\phi^{(o)}$ at the midpoints of C_j and designate them by $\phi_{jN}^{(e)}$ and $\phi_{jN}^{(o)}$, then due to the property of the surface distribution of source[16], we have

$$\phi_{iN}^{(e)} \equiv f_i^{(e)} = \frac{Q_i^{(e)}}{2} + \sum_{\substack{k=1 \\ k\neq i}}^{M} Q_k \int_{C_k} G_N^{(e)}(l;y_i,z_i)dl \qquad (I\text{-}11)$$

$$\phi_{iN}^{(o)} \equiv f_i^{(o)} = \frac{Q_i^{(o)}}{2} + \sum_{\substack{k=1 \\ k\neq i}}^{M} Q_k \int_{C_k} G_N^{(o)}(l;y_i,z_i)dl$$

These two equations can be expressed in algebraic form as

$$A^{(e)}Q^{(e)} = B^{(e)}$$

$$A^{(o)}Q^{(o)} = B^{(o)}$$

where $A^{(e)}$ and $A^{(o)}$ are M by M matrices, the elements of which are given by

$$A_{ik}^{(d)} = \int_{C_k} G_N^{(d)}(l;y_i,z_i)dl \text{ for } (d) = (e) \text{ or } (o)$$

$Q^{(e)}$ and $Q^{(o)}$ are the column vectors, the elements of which are given by $Q_k^{(e)}$ and $Q_k^{(o)}$, respectively (however, if k=i, only half of the values should be taken), and $B^{(e)}$ and $B^{(o)}$ are the column vectors, the elements of which are given by $f_i^{(e)}$ and $f_i^{(o)}$, respectively.

Then, we can obtain the unknowns $Q^{(e)}$ and $Q^{(o)}$ by

$$Q^{(d)} = \left[A^{(d)}\right]^{-1}B(d) \text{ for } (d) = (e) \text{ or } (o)$$

and substitution of these into Equations (I-8) and (I-9) yields $\phi^{(e)}$ and $\phi^{(o)}$.

For the diffraction potential ϕ_D', we have

$$f \equiv f^{(e)} + f^{(o)} = -\frac{\partial}{\partial N}\left(\frac{jg\zeta_A}{\omega}e^{Kz-jKy\sin\mu}\right)\Big|_{C_0}$$

hence,

$$f^{(e)} = j\omega\zeta_A e^{Kz}[N_2\sin\mu\sin(Ky\sin\mu) - N_3\cos(Ky\sin\mu)]$$

$$f^{(o)} = -\omega\zeta_A e^{Kz}[N_2\sin\mu\cos(Ky\sin\mu) + N_3\sin(Ky\sin\mu)]$$

where (y,z) is a point on C_0 and N_2 and N_3 are respectively the y- and z-component of the unit vector on C_0 pointing into the body. For a symmetric body N_2 is an odd function of y and N_3 is an even function.

For the motion potential ϕ_k', we have the following boundary condition on C_0:

k	$f^{(e)}$	$f^{(o)}$
2	0	$j\omega_e N_2$
3	$j\omega_e N_3$	0
4	0	$j\omega_e N_4$

where $N_4 = yN_3 - zN_2$.

Appendix II

Irregular Frequencies

It is well known that the Green's function method[9] for the velocity potential function associated with an oscillating body in a free surface suffers from the existence of indefinite solutions at certain discrete frequencies. These frequencies are often referred to as "irregular frequencies." John[9] showed that they are equivalent to the eigenvalues of the boundary-value problem for the velocity potential defined in the internal fluid domain bounded by the body surface and the interior line $z = 0$. That is, if the velocity potential $\tilde{\phi}$ defined inside the body has nontrivial solutions for the boundary condition

$$\tilde{\phi}_z - \lambda\tilde{\phi} = 0 \quad \text{on } C_f(z = 0, -b < y < b)$$
$$\tilde{\phi} = 0 \quad \text{on } C_0 \tag{II-1}$$

for discrete values of λ, then $\omega_l = \sqrt{g\lambda_l}$ is the lth irregular frequency for $l = 1, 2, \ldots$

If the velocity potential ϕ defined in the fluid region R outside the body is expressed by

$$\phi(p) = \int_{C_0} Q(1)G(1;p)\,dl, \tag{II-2}$$

then

$$f(p_0) \equiv \phi_N(p)\Big|_{p\to p_0} = \pi Q(p_0) + \int_{C_0} Q(1)G_N(i;p_0)\,dl \tag{II-3}$$

where $f(p_0)$ is prescribed. The Fredholm theorem states that Q has a unique solution if the associated homogeneous equation, i.e., $f = 0$ in Equation (II-3), has a trival solution only. From John's uniqueness proof[9] we know that if $\phi_N|_{C_0} = 0$, ϕ identically vanishes in R and on C_0. Since ϕ given by Equation (II-2) is continuous everywhere in $z \le 0$, it can be extended to the interior domain R'. If we let $\tilde{\phi}(p') = \int_{C_0} Q(1)G(1;p'\in R')\,dl$, $\tilde{\phi}$ should have trivial solutions for the boundary condition (II-1) if ϕ is unique. But, the fact that for some λ_l, $\tilde{\phi}$ has nontrivial solutions implies that $\tilde{\phi}_N|_{p\to p_0} \neq 0$; hence, $Q(1) = \tilde{\phi}_N(1) \neq 0$ on C_0 if $\lambda = \lambda_l$. The identity $Q(1) = \tilde{\phi}_N(1)$ can be easily proved. From Green's theorem we can show for any point p in the interior domain R' bounded by C_0 and C_f that

$$\tilde{\phi}(p') = \int_{C_0} [\tilde{\phi}_N G(p') - \tilde{\phi}G_N]\,dl,$$
$$0 = \int_{C_0} [\phi_N G(p') - \phi G_N]\,dl, \tag{II-4}$$

hence, subtracting the two equations above, we get

$$\tilde{\phi}(p') = \int_{C_0} [(\tilde{\phi}_N - \phi_N)G(p') - (\tilde{\phi} - \phi)G_N]\,dl$$
$$= \int_{C_0} \tilde{\phi}_N G(p')\,dl \tag{II-5}$$

since $\phi = \tilde{\phi} = \phi_N = 0$ on C_f, and from Equations (II-4) and (II-5) we find that $\tilde{\phi}_N(1) = Q(1)$. Since Q(1) cannot be identically zero on C_0, the associated homogeneous equation of (II-3) can have nontrivial solutions at $\lambda = \lambda_j$.

Frank[10] has shown that the added mass and damping coefficients of cylindrical bodies have discontinuities at certain discrete frequencies. Several investigators have shown either in published[11,17,18] or unpublished forms various methods for alleviating the irregular frequencies. The removal of the irregular frequencies is achieved in this work by imposing $\phi_z' = 0$ or $\phi' = 0$ on the interior waterline C_f. This imposed boundary condition on C_f then makes $\tilde{\phi} \equiv 0$ in R' since

$$\iint_{R'} |\nabla\tilde{\phi}|^2\,ds = \int_{C_0+C_f} \tilde{\phi}\,\tilde{\phi}_N\,dl = 0 \tag{II-6}$$

for $\tilde{\phi}|_{C_0} = 0$ and $\tilde{\phi}_N|_{C_f} = 0$ and, therefore, $|\nabla\tilde{\phi}| = 0$ in R' implies that $\tilde{\phi} \equiv 0$.

With this approach we can begin with a new definition of ϕ' by

$$\phi'(p) = \int_{C_0+C_f} Q(1)G(1;p)\,dl$$

and solve for Q from the Fredholm equation

$$f(p_0) = \phi_N'(p_0) = \pi Q(p_0) + \int_{C_0+C_f} Q(1)G_N(1;p_0)\,dl$$

with

$$\phi_N'\Big|_{C_f} = \phi_z'\Big|_{C_f} = 0.$$

References

1. Gerzina, D.M. and E.L. Woo, "CVA 68 Relative Motion Investigation," DTNSRDC Report SPD-656-01, Dec. 1975.

2. Bales, N.K., et al., "Validity of a Strip Theory-Linear Superposition Approach to Predicting Probability of Deck Wetness for a Fishing Vessel," DTNSRDC Report SPD-643-01, Nov. 1975.

3. Cox, G.G. and D.M. Gerzina, "A Comparison of Predicted Experimental Seakeeping Characteristics for Ships with and without Large Bow Bulbs," DTNSRDC Report SPD-591-01, Nov. 1974.

4. Salvesen, N., et al., "Ship Motion and Sea Loads," SNAME Trans., Vol. 78, 1970.

5. Wehausen, J. and E.V. Laitone, "Surface Waves," Encyclopedia of Physics, Vol. 9, Springer-Verlag, 1960.

6. Ursell, F., "The Expansion of Water-Wave Potentials at Great Distances," Proc. Camb. Phil. Soc., Vol. 64, pp. 811-826, 1968.

7. Choo, K.Y., "Exciting Forces and Pressure Distribution on a Ship in Oblique Waves," Ph.D. Thesis at MIT, Ocean Eng. Dept., 1975.

8. Troesch, A.W., "The Diffraction Potential for a Slender Ship Moving Through Oblique Waves," Univ. of Mich., NAME Dept., Report No. 176, Feb. 1976.

9. John, F., "On the Motion of Floating Bodies: II. Simple Harmonic Motions," Commun. Pure Appl. Math., Vol. 13, pp. 45-101, 1950.

10. Frank, W., "Oscillation of Cylinders in or below the Free Surface of Deep Fluids," NSRDC Report 2375, 1967.

11. Ohmatsu, S., "On the Irregular Frequencies in the Theory of Oscillating Bodies in a Free Surface," Papers of Ship Res. Inst. (Japan) No. 48, 1975.

12. Newman, J.N., "The Exciting Forces on Fixed Bodies in Waves," J. Ship Res., Vol. 6, No. 3, 1962.

13. Abramowitz, M. and I.A. Stegun (Ed.), "Handbook of Mathematical Functions," National Bureau of Standards, Appl. Math. Ser. 55, 1964.

14. Todd, J., "Evaluation of the Exponential Integral for Large Complex Arguments," J. Research NBS 52, RP. 2508, pp. 313-317, 1954.

15. Hastings, C. Jr., "Approximations for Digital Computers," Princeton Univ. Press, Princeton, N.J., 1955.

16. Kellog, O.D., "Foundation of Potential Theory," Dover Publications, Inc., New York, 1953 (see p. 164).

17. Pien, P.C. and C.M. Lee, "Motion and Resistance of a Low-Waterplane Catamaran," The Ninth Symposium on Naval Hydrodynamics, Vol. 1, U.S. Government Printing Office, 1972.

18. Ogilvie, T.F. and Y.S. Shin, "Integral-Equation Solution for Time-Dependent Free-Surface Problems," J. of Soc. of Naval Arch. of Japan, Vol. 143, pp. 41-51, 1978.

INITIAL DISTRIBUTION

Copies	
1	CHONR
	1 LIB
1	NRL (LIBRARY)
5	NAVSEA
	1 03R2
	1 32131
	1 32132
	1 32133
	1 31211 (KENNEL)
2	USNA
	1 LIB
	1 BHATTACHARYYA
1	NAVPGSCOL LIB
1	NROTC & NAVADMINU, MIT
1	NADC
1	NOSC (LIBRARY)
12	DTIC
2	HQS COGARD
1	MARAD
2	MMA
	1 LIB
	1 DR. MCCLEAN
1	NSF ENGR DIV LIB
2	U CAL BERKELEY/DEPT NAOF
	1 NAOF LIB
	1 WEHAUSEN
1	FLORIDA ATLANTIC U OE LIB
2	U HAWAII/BRETSCHNEIDER
3	MIT
	1 BARKER ENG LIB
	1 OCEAN ENGR/SCLAVOUNOS
	1 OCEAN ENGR/YEUNG

Copies	
1	ORI, INC
	1 KIM
1	ST JOHNS U
	1 HSIEUNG
1	SWRI
	1 APPLIED MECH REVIEW
1	BOEING ADV AMR SYS DIV
1	SIT DAVIDSON LAB
	1 LIB
2	WEBB INST
	1 WARD
	1 HADLER
1	SNAME
1	HYDRONAUTICS
1	SCIENCE APPLICATIONS, INC./ ANNAPOLIS
	1 SALVESEN
1	UNIV WASHINGTON
	1 MECH ENGR/ADEE
1	MARITIME RES INF SERVICE
2	U MICHIGAN ANN ARBOR/DEPT NAME
	1 BECK
	1 TROESCH

CENTER DISTRIBUTION

Copies	Code	Name
1	1113	Lamb
1	1115	Allen
1	1504	Monacella
1	156	Cieslowski
1	1506	Fine

CENTER DISTRIBUTION (Continued)

Copies	Code	Name
1	152	Lin
1	1521	Day
1	1522	Wilson
10	1522	Kim
1	1523	Koh
1	154	McCarthy
10	1542	Lee
1	1542	Huang
1	1542	Bai
1	1542	Chang
1	154	Yim
1	1561	O'Dea
1	1561	McCreight
1	1562	Hong
1	1562	McCreight
1	1562	Moran
1	1563	Russ
1	1843	Haussling
10	5211.1	Reports Distribution
2	522.1	Unclassified Lib (C) (m)
1	522.2	Unclassified Lib (A)

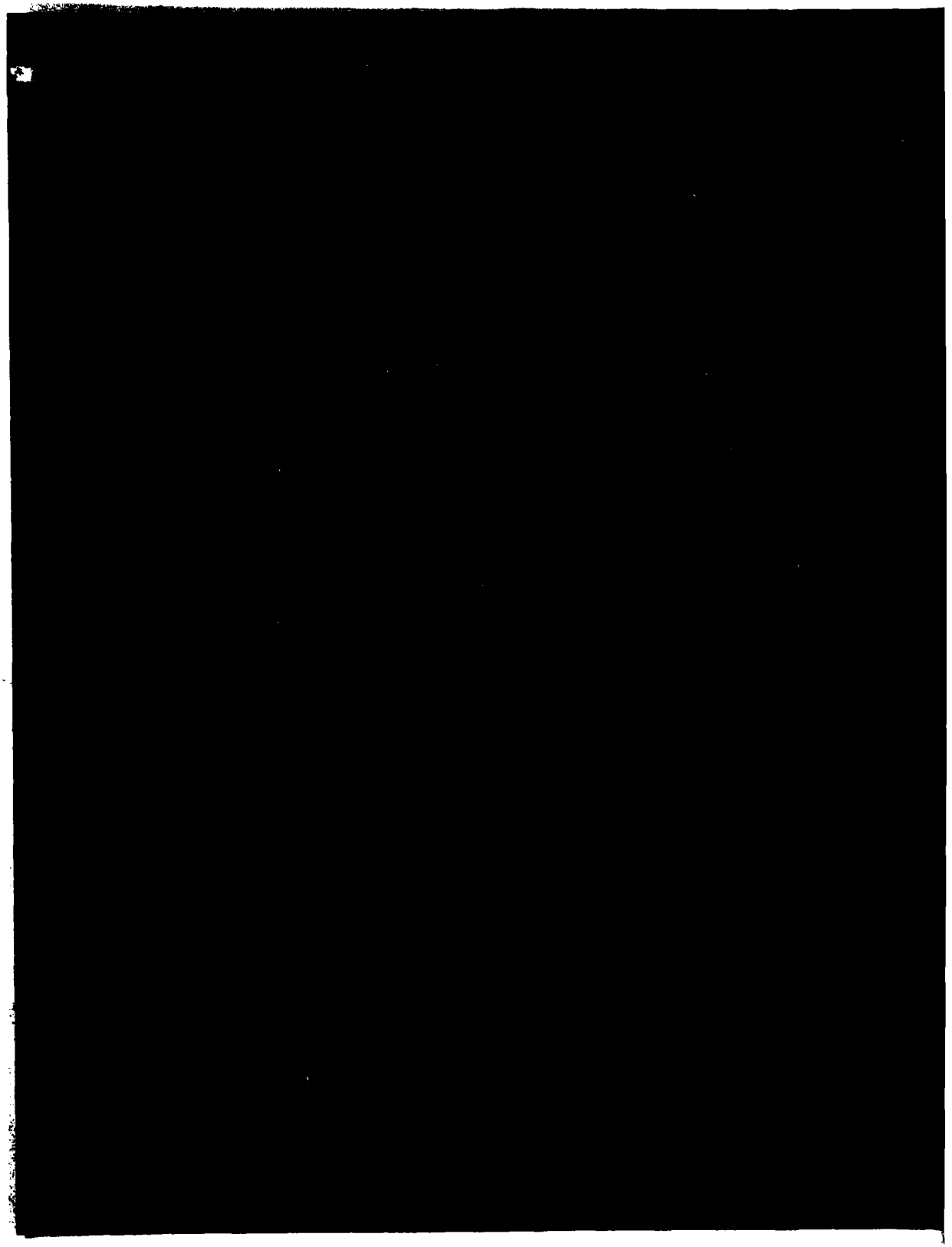


DAT
FILM